

Thermalization of a pump-excited Mott insulator

Martin Eckstein¹ and Philipp Werner¹

¹*Theoretical Physics, ETH Zurich, 8093 Zurich, Switzerland*

(Dated: October 31, 2018)

We use nonequilibrium dynamical mean-field theory in combination with a recently implemented strong-coupling impurity solver to investigate the relaxation of a Mott insulator after a laser excitation with frequency comparable to the Hubbard gap. The time evolution of the double occupancy exhibits a crossover from a strongly damped transient at short times towards an exponential thermalization at long times. In the limit of strong interactions, the thermalization time is consistent with the exponentially small decay rate for artificially created doublons, which was measured in ultracold atomic gases. When the interaction is comparable to the bandwidth, on the other hand, the double occupancy thermalizes within a few times the inverse bandwidth along a rapid thermalization path in which the exponential tail is absent. Similar behavior can be observed in time-resolved photoemission spectroscopy. Our results show that a simple quasi-equilibrium description of the electronic state breaks down for pump-excited Mott insulators characterized by strong interactions.

I. INTRODUCTION

State-of-the-art pump-probe experiments use ultrashort light pulses to control and probe the complex interplay between electronic, magnetic and lattice degrees of freedom in strongly correlated materials.^{1–6} The Mott metal-insulator transition, which is the paradigm for phase transitions in correlated electron systems, has been investigated in several time-resolved experiments. For example, a photo-induced metal-insulator transition and the ultrafast recovery of the Mott gap was observed in a charge-transfer insulator by using reflectivity measurements,¹ and in 1T-TaS₂ using time-resolved photoemission spectroscopy.² Recently, Wall *et al.* succeeded in measuring electronic dynamics in an organic charge-transfer insulator on the timescale of the inverse bandwidth \hbar/W .⁴

Photo-excited phases in materials with several competing interactions have been reached along nonthermal pathways,³ and their properties can be quite different from those of any known equilibrium state of the same system.^{5,6} On the other hand, in many experiments the electronic state has been interpreted in terms of the two-temperature model,⁷ whose basic assumption is that electrons thermalize rapidly (on the timescale of the inverse bandwidth) and thereafter can be assigned a temperature which is different from the lattice temperature. Deviations from the two-temperature behavior have been observed long ago in noble metals, where the scattering between quasiparticles is weak and thermalization times can range up to a few hundred femtoseconds.⁸ In strongly interacting quantum systems, thermalization is theoretically not well understood, and it is thus unclear whether a homogeneous electron system can be stuck in a nonthermal state on timescales much longer than \hbar/W .

Nonequilibrium experiments on ultracold atomic gases^{9,10} have recently stimulated considerable theoretical effort to resolve some of the questions related to the thermalization of isolated quantum-many body systems.¹¹ In several models^{12–15} it was found that the

relaxation after a sudden quench of the Hamiltonian sensitively depends on the interaction parameter. In the fermionic Hubbard model, e.g., rapid thermalization of the momentum distribution (within $t \sim \hbar/W$) occurs after quenches from the noninteracting ground state to a very narrow interaction regime at intermediate coupling ($U \approx 0.8W$ for the semi-elliptic density of states),¹⁴ while after quenches to weak and strong coupling one observes the formation of a quasistationary nonthermal state which persists for $t \gg \hbar/W$.^{14–16} The latter phenomenon, which is called prethermalization, can be related to the non-ergodic behavior of integrable models,¹⁷ because in both cases the dynamics is constrained by either exact or approximate constants of motion.¹⁸

In this paper we turn from interaction quenches to the pump-probe setup and study the relaxation of a Mott insulator after a short laser excitation. The analysis is performed for the Hubbard model,

$$H = \sum_{ij, \sigma=\uparrow, \downarrow} t_{ij} c_{i\sigma}^\dagger c_{j\sigma} + U \sum_i (n_{i\uparrow} - \frac{1}{2})(n_{i\downarrow} - \frac{1}{2}), \quad (1)$$

which describes fermionic particles that can hop between the sites of a crystal lattice (with hopping amplitude t_{ij}) and interact with each other through a local Coulomb repulsion U . In the phase diagram of the Hubbard model there is a metal-insulator transition at low temperatures and half-filling ($n_\uparrow = n_\downarrow = \frac{1}{2}$). For the present investigation we focus on higher temperatures, where this phase transition turns into a smooth crossover, and study the relaxation after a short pump-pulse that excites carriers over the Mott gap. Although the equilibrium states before the excitation are then continuously connected, the response to the pulse turns out to be strongly dependent on the value of U .

For all values of U , the system approaches a thermal state, which is at elevated temperature because the energy is increased during the pump and conserved thereafter. However, just as for the interaction quench¹⁴ the thermalization time τ_{th} depends sensitively on U . Already for moderately strong interactions, where the Hubbard gap is still comparable to the bandwidth, τ_{th} is much

larger than \hbar/W , which puts a question mark behind the applicability of a simple two-temperature model in this case. At intermediate coupling, on the other hand, thermalization indeed happens on the timescale of the inverse bandwidth, but it then follows a qualitatively different path which may be referred to as “rapid thermalization”.

To study the dynamics of the Hubbard model, we use the dynamical mean-field theory,¹⁹ which provides a mapping of the lattice model onto a single impurity model and is exact in the limit of infinite dimensions.²⁰ The reformulation of DMFT within the Keldysh framework^{21,22} allows to apply this approach to nonequilibrium problems in which a system is initially prepared in a thermal equilibrium state and subsequently exposed to some perturbation. The biggest challenge for the method is the solution of a quantum impurity model under quite general nonequilibrium conditions. A generalization of the auxiliary-field weak-coupling continuous-time quantum Monte Carlo method²³ has been used successfully to study the short-time dynamics of the Hubbard model,^{14,15,24,25} but the dynamical sign problem prevents an investigation of the long-time behavior, in particular for large values of U which are of interest for the current investigation of Mott-insulating states. Possibilities to avoid the difficulties of real-time Monte Carlo methods include the superperturbation theory,²⁶ and perturbative approaches.^{15,27} For the present study we use the self-consistent strong-coupling expansion,²⁷ which is a generalization of the non-crossing approximation²⁸ (NCA) to higher orders and to the Keldysh contour. It works particularly well in the Mott insulating phase, and the comparison of results from different orders (up to third order) provides at least some estimate of the error.

The outline of this paper is as follows: In Section II we give some details of the DMFT framework used here, in particular the solution of the lattice Dyson equation in real (Keldysh) time. We then present results for the relaxation of the double occupancy after a pump-excitation of a Mott insulator (Sec. III) and identify the corresponding signatures in time-resolved photoemission spectroscopy (Sect. IV). A conclusion is given at the end (Sec. V).

II. THE MODEL

A. Hubbard Model in an external electric field

In this paper we investigate the Hubbard model with an additional spacially homogeneous, but time-dependent electric field,

$$\mathbf{E}(t) = \hat{\mathbf{n}} E_0 \sin(\Omega t) \phi(t), \quad (2)$$

corresponding to a few-cycle pump-pulse with amplitude E_0 , polarization $\hat{\mathbf{n}}$, frequency Ω , and a pulse envelope $\phi(t)$. (The assumption of spacial homogeneity is appropriate for optical frequencies with wavelength much

larger than the lattice spacing.) Within a gauge without scalar potential, \mathbf{E} is determined by the vector potential through the relation $\mathbf{E} = -\frac{1}{c}\partial_t\mathbf{A}$, and the latter is incorporated into the Hamiltonian (1) via a Peierls substitution in the hopping amplitudes t_{ij} . This leads to a shift of the band energies $\epsilon_{\mathbf{k}}$, i.e., the hopping part of Eq. (1) becomes time-dependent,

$$H(t) = \sum_{\mathbf{k}\sigma} h_{\mathbf{k}}(t) n_{\mathbf{k}\sigma} + U \sum_i (n_{i\uparrow} - \frac{1}{2})(n_{i\downarrow} - \frac{1}{2}), \quad (3)$$

with $h_{\mathbf{k}}(t) = \epsilon_{\mathbf{k} - \frac{e}{\hbar c}\mathbf{A}(t)}$. In the following we choose a hypercubic lattice in the limit of infinite dimensions with a Gaussian density of states

$$\rho(\epsilon) = \frac{1}{\sqrt{\pi}W} \exp\left(-\frac{\epsilon^2}{W^2}\right). \quad (4)$$

The unit for energy is given by the variance W of the density of states, which will be loosely referred to as the bandwidth, time is measured in units of \hbar/W , and the unit of the electric field is given by W/ea , where $-e$ is the electronic charge and a is the lattice spacing. In these units, the critical end-point of the first-order Mott transition line in the phase diagram of the paramagnetic half-filled Hubbard model, which is obtained quite accurately at second order in the self-consistent hybridization expansion,²⁷ is located at $U \approx 3.1$ and $T \approx 0.02$.

The DMFT equations for this setup have been discussed in detail in Ref. 22 for a polarization $\hat{\mathbf{n}} = (1, 1, \dots, 1)^t$ along the body diagonal of the cubic unit cell, and they will not be repeated in detail. Because $\mathbf{A}(t)$ enters in the effective impurity action only indirectly via the hybridization function, we can apply the self-consistent hybridization expansion as an impurity solver without modifications.²⁷ If not stated otherwise we use the second order of that approximation as an impurity solver (one-crossing approximation, OCA), which is reliable in the insulating phase and in the crossover regime.²⁷

B. Solution of the DMFT self-consistency

Within the DMFT framework, a repeated solution of the lattice Dyson equation and the Dyson equation of the impurity model is required (for details, see, e.g., Refs. 22 and 15). These equations are in essence integro-differential equations on the Keldysh contour \mathcal{C} which runs from 0 to time t_{\max} (i.e., the largest time of interest) along the real axis, back to 0, and finally to $-i\beta$ along the imaginary time axis.²⁹ Since there are in principle several ways to rephrase and solve these equations, we use the remaining paragraphs of this section to describe a scheme which we found to be reliable. The same scheme has been used previously to study the dielectric breakdown of the Mott insulator.³⁰

The following approach is mainly designed to satisfy two properties: (i) It is easy to implement a higher order scheme in the timestep Δt to reduce the discretization

error. We found that this considerably increases the accuracy for a given number of timesteps N on \mathcal{C} , which in turn strongly reduces the required storage [$\mathcal{O}(N^2)$] and computational effort [$\mathcal{O}(N^3)$ for NCA, $\mathcal{O}(N^4)$ for OCA]. (ii) The approach exactly satisfies the causal structure of the equations, i.e., the solution at a given time is computed using only information from previous times. This makes the solution of the nonequilibrium DMFT equations equivalent to a time-propagation that starts from the initial equilibrium DMFT solution, rather than an iteration of the equations on the full contour \mathcal{C} .

To design such a scheme we rewrite the integro-differential equations on \mathcal{C} explicitly for the imaginary-time, real-time, and mixed imaginary-time/real-time components of the two-time propagators $G(t, t')$. This step has been described in detail in Ref. 15. The resulting equations are integral equations of Volterra type, whose solution can be easily designed in a way to satisfy the requirements (i) and (ii) above. We found that two types of integral equations are particularly well-behaved (both are to be solved for \mathbf{X}): The integral equation

$$(\mathbf{I} - \mathbf{A}) * \mathbf{X} = \mathbf{B}, \quad (5)$$

and the integro-differential equation (basically a Dyson equation)

$$[i\partial_t - \mathbf{h} - \mathbf{A}] * \mathbf{X} = \mathbf{I}, \quad (6)$$

where $\mathbf{h}(t, t') = \delta_{\mathcal{C}}(t, t')h(t)$ is a function of the physical time t only. Here and in the following, bold quantities $\mathbf{X}(t, t')$ denote two-time functions with arguments on \mathcal{C} , $[\mathbf{A} * \mathbf{B}](t, t') = \int_{\mathcal{C}} d\bar{t} \mathbf{A}(t, \bar{t})\mathbf{B}(\bar{t}, t')$ is the contour convolution, and $\mathbf{I}(t, t') = \delta_{\mathcal{C}}(t, t')$ is the delta function on \mathcal{C} . When written as explicit integral equations for the real and imaginary-time components, Eq. (5) leads to Volterra equations of the second kind. In contrast, the slightly modified equation $\mathbf{A} * \mathbf{X} = \mathbf{B}$ leads to Volterra equations of the first kind, which tend to be unstable for high-order algorithms. In the remainder of this section we show how to rewrite the DMFT selfconsistency equations (appropriate for the NCA-type impurity solver) only in terms of equations of type (5).

Nonequilibrium DMFT corresponds to a self-consistent solution of the following set of equations: (i) Solution of the impurity problem, which in the case of the strong-coupling expansion requires an evaluation of the diagrammatic expression for the local Greenfunction in terms of the hybridization function $\mathbf{\Lambda}$,²⁷

$$\mathbf{G} = \mathbf{G}_{NCA, \dots}[\mathbf{\Lambda}], \quad (7)$$

(ii), the Dyson equation of the impurity model

$$[i\partial_t + \mu - \Sigma - \mathbf{\Lambda}] * \mathbf{G} = \mathbf{I}, \quad (8)$$

(iii), the lattice Dyson equation with the time-dependent band-energies $h_{\mathbf{k}}(t)$ from Eq. (3)

$$[i\partial_t + \mu - \Sigma - \mathbf{h}_{\mathbf{k}}] * \mathbf{G}_{\mathbf{k}} = \mathbf{I}, \quad (9)$$

and (iv), the momentum sum

$$\sum_{\mathbf{k}} \mathbf{G}_{\mathbf{k}} = \mathbf{G}. \quad (10)$$

To reformulate this set of equations only in terms of equations of type (5) we introduce the quantity $\mathbf{Z} = [i\partial_t + \mu - \Sigma]^{-1}$, conjugate to the self-energy, and the momentum sums $\mathbf{G}_1 = \sum_{\mathbf{k}} \mathbf{h}_{\mathbf{k}} \mathbf{G}_{\mathbf{k}}$, $\mathbf{G}_1^{\dagger} = \sum_{\mathbf{k}} \mathbf{G}_{\mathbf{k}} \mathbf{h}_{\mathbf{k}}$, and $\mathbf{G}_2 = \sum_{\mathbf{k}} \mathbf{h}_{\mathbf{k}} \mathbf{G}_{\mathbf{k}} \mathbf{h}_{\mathbf{k}}$ in addition to Eq. (10). By summing Eq. (9) over \mathbf{k} (using $\sum_{\mathbf{k}} \mathbf{h}_{\mathbf{k}} = 0$) and comparing with Eq. (8) one can show that $\mathbf{G}_1 = \mathbf{\Lambda} * \mathbf{G}$, $\mathbf{G}_1^{\dagger} = \mathbf{G} * \mathbf{\Lambda}$, and that Eqs. (8)-(10) are equivalent to

$$[\mathbf{I} + \mathbf{G}_1^{\dagger}] * \mathbf{Z} = \mathbf{G}, \quad (11)$$

$$[\mathbf{I} - \mathbf{F}_{\mathbf{k}}] * \mathbf{G}_{\mathbf{k}} = \mathbf{Z}, \quad (12)$$

$$[\mathbf{I} + \mathbf{G}_1] * \mathbf{\Lambda} = \mathbf{G}_2, \quad (13)$$

where $\mathbf{F}_{\mathbf{k}}(t, t') = \mathbf{Z}(t, t')h_{\mathbf{k}}(t')$. In practice, we determine \mathbf{G} from $\mathbf{\Lambda}$ via the self-consistent hybridization expansion, perform the convolution $\mathbf{G} * \mathbf{\Lambda}$ to obtain an estimate for \mathbf{G}_1^{\dagger} , then solve Eq. (11) for \mathbf{Z} , Eq. (12) for $\mathbf{G}_{\mathbf{k}}$ on a given set of \mathbf{k} -points, perform the momentum sums to obtain \mathbf{G} , \mathbf{G}_1 , \mathbf{G}_1^{\dagger} , and \mathbf{G}_2 , and finally solve Eq. (13) for $\mathbf{\Lambda}$. This cycle is performed consecutively for each timestep (starting from an extrapolation of $\mathbf{\Lambda}$ from the previous timestep), which usually does not require more than two or three iterations to reach a converged solution.

III. THERMALIZATION OF THE PUMP-EXCITED MOTT INSULATOR

In this section we analyze the dynamics of Mott-insulating and crossover states in the half-filled Hubbard model after pump-pulses with frequencies of the order of the gap. The system is initially prepared in an equilibrium state at given temperature $T = 1/\beta$, and excited by a few-cycle electrical field pulse [Eq. (2)] that has a Gaussian pulse envelope $\phi(t) = \exp[-(t-2)^2]$ and is restricted to time $0 \leq t \leq 4$ (Fig. 1a). Figure 1b shows the typical time dependence of the total energy $\mathcal{E}(t) = \langle H(t) \rangle$ during and after the pump-excitation for an initially Mott-insulating state ($U = 5$, $\beta = 5$). During the pump, $\mathcal{E}(t)$ increases with time due to the absorption of light, while it is constant or $t > 4$ because the system is not coupled to external thermal reservoirs. Note that energy conservation comes out correct only if all approximations that are made for the solution of the impurity model are conserving in the sense of Kadanoff and Baym, which is true for the self-consistent hybridization expansion. More precisely, energy conservation implies the relation $\dot{\mathcal{E}}(t) = \mathbf{E}(t) \langle \mathbf{j}(t) \rangle$, which can serve as a first check for the numerics ($\mathbf{j} = e \sum_{\mathbf{k}\sigma} n_{\mathbf{k}\sigma} \mathbf{v}_{\mathbf{k}}$ is the current operator, with band velocities $\mathbf{v}_{\mathbf{k}} = \hbar^{-1} \partial_{\mathbf{k}} \epsilon_{\mathbf{k} - \frac{e}{\hbar c} \mathbf{A}}$).

It is the basic assumption of the two-temperature model that due to the electron-electron interaction elec-

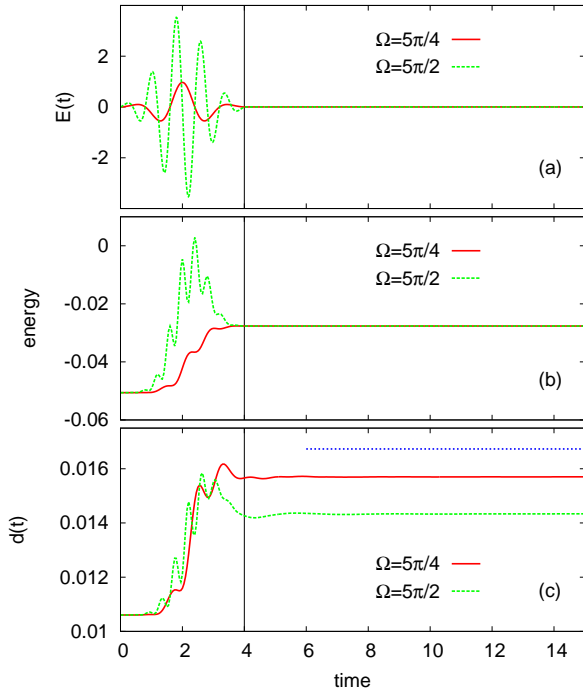


FIG. 1: Pump-excitation of a Mott insulator at $\beta = 5$, $U = 5$. a) The electric field used for the data of this plot. The two frequencies $\Omega = 5\pi/4 \approx 3.927$ and $\Omega = 5\pi/2 \approx 7.854$ are comparable to the Hubbard gap and larger than the Hubbard gap, respectively, and the amplitudes $E_0 = 0.9679$ ($\Omega = 5\pi/4$) and $E_0 = 3.6701$ ($\Omega = 5\pi/2$) are chosen such that $T_{\text{eff}} = 0.5$, i.e., the energy of the pump-excited system for $t > 4$ is the same as in a system in thermal equilibrium at temperature $T = T_{\text{eff}}$. b) Time-dependence of the total energy \mathcal{E} . c) Time dependence of the double occupancy $d(t)$. The horizontal dotted line indicates the double occupancy $d(T_{\text{eff}})$ in an equilibrium state at temperature $T = T_{\text{eff}}$.

trons in a solid thermalize so fast that the lattice dynamics is not important for that process. In the present case, thermalization implies that the time-evolved state has the same properties as the uniquely defined thermal equilibrium state whose temperature is such that its energy equals the energy of the pump excited system, $\mathcal{E}(t > 4) = \text{Tr}[e^{-H/T_{\text{eff}}}H]/Z$. The latter condition defines an effective temperature $T_{\text{eff}}(\mathcal{E})$, and we test for thermalization by comparing time-dependent expectation values of observables $\mathcal{O}(t)$ to thermal expectation values $\mathcal{O}(T_{\text{eff}}) = \text{Tr}[e^{-H/T_{\text{eff}}}\mathcal{O}]/Z$ which are obtained from an independent equilibrium DMFT calculation. To compute the thermal energy $\mathcal{E}(T) = \text{Tr}[e^{-H/T}H]/Z$ which is needed for the determination of T_{eff} , we use the same impurity solver as in the nonequilibrium calculation, i.e., the same order of the self-consistent hybridization expansion.

In Fig. 1c we compare thermal and time-dependent expectation values of the double occupancy $d(t) = \langle n_{i\uparrow}n_{i\downarrow} \rangle$, which is a purely local quantity and can be measured di-

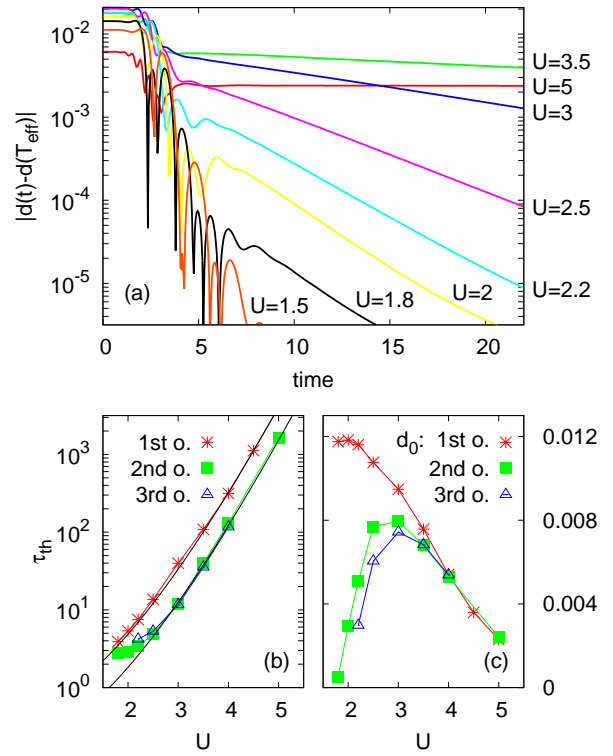


FIG. 2: Relaxation of the double occupancy $d(t)$ after an excitation with frequency $\Omega = U\pi/2$ ($\beta = 5$). Upper panel: (a) The difference $|d(t) - d(T_{\text{eff}})|$, obtained from the OCA impurity solver. The pump-amplitudes E_0 are given by 3.6701 ($U = 5$), 2.4397 ($U = 3.5$), 2.1325 ($U = 3$), 1.9123 ($U = 2.5$), 1.8198 ($U = 2.2$), 1.7761 ($U = 2$), 1.6632 ($U = 1.8$), 1.2765 ($U = 1.5$), such that $T_{\text{eff}} = 0.5$ in all cases. Lower panels: Parameters τ_{th} (b) and d_0 (c), obtained from fitting the curves in a) for $t > 12$ with Eq. (14) (square symbols). Stars and triangles show the result of the analogous investigation using NCA and the 3rd order hybridization expansion, respectively. The time-evolution in 3rd order was restricted to $t \leq 15$. Black solid lines in b) correspond to the exponential law³² $\tau_{\text{th}} = \tau_0 \exp(\alpha U \log U)$, with $\alpha = 1.01$ and $\tau_0 = 0.45$ (1.2) for OCA (NCA).

rectly in the impurity model. Apparently, a large part of the excitation energy goes into the creation of doublon-holon pairs, such that $d(t)$ rises by more than 30% during the pump relative to its small value in the initial Mott-insulating state. Subsequent to the pump, $d(t)$ rapidly settles at a value $d_{\text{stat}} \neq d(T_{\text{eff}})$, and further relaxation towards the thermal value is hardly visible on the scale of Fig. 1. This behavior is similar to that of the Hubbard model after an interaction quench.¹⁴ However, a sudden change of the interaction causes pronounced $2\pi/U$ -periodic oscillations which have been used to characterize the short time behavior in Ref. 14, while these oscillations are very weak in the present case, where the pump-excitation itself takes already longer than the period $2\pi/U$.

The long-lived nonthermal value of $d(t)$ implies that doubly occupied and empty sites do not rapidly recombine in the Hubbard model at large Coulomb repulsion.^{31,32} In fact, in experiments with ultra-cold atoms it was found that for $U \gg W$ an artificially increased double occupancy relaxes only on the exponentially long timescale $\tau \propto \exp(\alpha \log(U/W)U/W)$,³² in agreement with theoretical predictions for the lifetime of a single doublon in a background of singly occupied sites and holes. The reason for this is that multi-particle scattering events are required to transform a large quantum of energy (U) into many kinetic energy excitations of a typical amount W , similar to the case of a semiconductor where electrons and holes cannot effectively recombine if the main relaxation channel is the emission of phonons with a much lower energy than the electronic band gap. The nonequilibrium DMFT approach now allows us to investigate how this decay rate of a single doublon is related to the thermalization of a “cloud” of many excitations, and how the relaxation is modified when U and W are comparable in magnitude.

To answer this question we plot the difference $|d(t) - d(T_{\text{eff}})|$ for a series of initial states at various values of the Coulomb interaction and temperature $T = 0.2$ (Fig. 2a). The pump frequency is $\Omega = \pi U/2$, and the pump amplitude E_0 is tuned such that the effective temperature after the pump is given by $T_{\text{eff}} = 0.5$. The time-evolution $d(t)$ is initially dominated by a damped transient, which subsequently turns into a smooth exponential relaxation towards the thermal value $d(T_{\text{eff}})$. The analysis of this exponential tail offers a rigorous way to separate the rapid short-time relaxation from the slower long-time thermalization: From a linear fit to the curves in Fig. 2a (for $t > 12$), i.e. an ansatz

$$d(t) \sim d(T_{\text{eff}}) + d_0 \exp(-t/\tau_{\text{th}}), \quad (14)$$

we extract both the long-time thermalization rate $1/\tau_{\text{th}}$, and a value d_0 which measures the “residue” of the initial rapid relaxation process. In the limit $U \gg W$, d_0 becomes identical to the apparent nonthermal stationary double occupancy d_{stat} introduced in the discussion of Fig. 1. The numerical effort required to resolve the small difference $d(t) - d(T_{\text{eff}})$ restricts the accessible times, such that a relaxation over more than one order of magnitude can be observed only for a limited range of interactions ($U = 2, 2.2, 2.5$ in Fig. 2). Nevertheless, the behavior of τ_{th} and d_0 as a function of U which is obtained on the basis of our present results already draws an interesting picture for the relaxation of the Hubbard model at strong and intermediate coupling, which we will discuss in the following two paragraphs.

For $U \gg W$, where the total number of excited doublons is small, we find that the dependence of the thermalization rate τ_{th} on U is indeed consistent with the exponential law³² $\tau_{\text{th}} = \tau_0 \exp(\alpha U \log U)$ that was predicted for the decay of a single doublon (Fig. 2b). Up to numerical accuracy, NCA, OCA, and the third order of the hybridization expansion give the same large- U

asymptotics for τ_{th} ($\alpha \approx 1$) and differ only by the prefactor τ_0 . Due to the exponential dependence on U , the thermalization rate is much larger than the inverse bandwidth already for moderately strong interactions.

When U and W are similar in magnitude, the relaxation changes in two ways: (i) the rate τ_{th} significantly decreases to values of the order of a few inverse W and starts to deviate from the large- U asymptotics, and (ii), the residue d_0 extrapolates to zero at a finite value of the interaction. While both facts eventually imply thermalization on a timescale given by the inverse bandwidth, they are conceptually quite different. The vanishing of the residue d_0 implies the absence of the long-time exponential relaxation tail, such that the system follows a qualitatively different path to the thermal state. In fact, the vanishing of the rapid relaxation residue d_0 provides a rigorous way to define a point of “rapid thermalization”, as opposed to a regular, two step relaxation. For $U < 1.5$ thermalization seems to become slower again, in agreement with similar findings for the interaction quench to the weak-coupling regime,^{14,16} but due to the limited numerical accuracy we cannot fit an exponential tail to the curves for $U < 1.8$ and study this regime systematically. That the system approaches a rapid thermalization point in the current setup may come as a surprise, because neither the sequence of initial states at $T = 0.2$, nor that of the final states at $T = 0.5$ crosses a known phase-transition of the half-filled Hubbard model. The phenomenon is clearly beyond a simple quasi-equilibrium explanation, and it is an interesting question whether it is related to the “rapid thermalization” at the dynamical transition in the Hubbard model after an interaction quench,¹⁴ and whether the latter can be characterized in a similar way.

IV. TIME-RESOLVED PHOTOEMISSION SPECTROSCOPY

The results of the previous section raise the question how well the different thermalization behaviors at strong and intermediate coupling can be distinguished by means of spectroscopic methods. In this section we will investigate this question for the case of time-resolved photoemission spectroscopy. The signal $I(\omega, t_p)$ in this case is simply defined as the probability for an electron to get emitted into an outgoing state with kinetic energy $\hbar\mathbf{k}^2/2m = \hbar\omega_{\text{probe}} - \omega - \Phi$ in response to a probe-pulse with frequency ω_{probe} at the probe-time t_p (Φ is the unknown work-function). Similar to equilibrium, the photoemission spectrum can be related to the single-particle Greenfunction $G^<(t, t') = i\langle c_{j\sigma}^\dagger(t')c_{j\sigma}(t) \rangle$ on a lattice site j ,³³

$$I(\omega, t_p) = -i \int dt dt' S(t)S(t') e^{i\omega(t'-t)} G^<(t_p + t, t_p + t'), \quad (15)$$

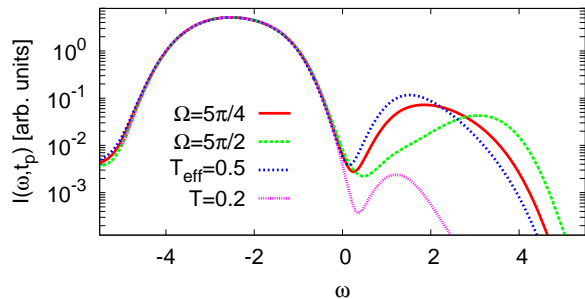


FIG. 3: Time-resolved photoemission spectrum [Gaussian probe, $\delta = 2$, $t_p = 10$] of a pump-excited system ($U = 5$, $\beta = 5$), using the pump parameters of Fig. 1. The blue dotted line marked $T_{\text{eff}} = 0.5$ is the photoemission spectrum of a system at temperature $T = 0.5$, for the same Gaussian probe pulse as for the other two curves.

where $S(t)$ is the envelope of the probe pulse. For the following investigation we use a Gaussian probe $S(t) = \exp(-t^2/2\delta^2)\Theta(3\delta - |t|)$, where δ is the duration. We cut off the exponential tails of the probe for $|t| > t_c = 3\delta$, such that Eq. (15) can be evaluated for probe times $t_c \leq t_p \leq t_{\text{max}} - t_c$ if the Greenfunction is known for $0 \leq t, t' \leq t_{\text{max}}$.

For the derivation of Eq. (15) one has to disregard matrix element effects and use the sudden approximation, which neglects the interaction between electrons in the outgoing states and in the solid.³³ These approximations are the same that are commonly made in order to compare photoemission spectra in equilibrium to the product of the spectral function $A(\omega)$ and the Fermi function $f(\omega)$. In fact, for an equilibrium state, $G^<(t, t')$ is just given by the Fourier transform $G^<(t, t') = i \int d\omega A(\omega) f(\omega) e^{i\omega(t'-t)}$, such that Eq. (15) is reduced to a convolution of the product $A(\omega)f(\omega)$ with the power density $|\tilde{S}(\omega)|^2 = |\int dt S(t) e^{i\omega t}|^2$ of the probe envelope $S(t)$, i.e., $I(\omega) = \int d\omega' |\tilde{S}(\omega')|^2 A(\omega - \omega') f(\omega - \omega')$. Hence $A(\omega)$ can in principle be measured with arbitrary accuracy by choosing a sufficiently long probe-pulse. On the other hand, for the nonequilibrium case the intrinsic frequency-time uncertainty in Eq. (15) makes it impossible to measure (or even define) transport of spectral weight on the timescale of the inverse bandwidth.³⁴ In the present case, however, we will show that time-resolved photoemission can be used to identify the thermalization signatures that have been discussed in the previous section.

In Fig. 3 we reconsider the two pump-experiments of Fig. 1 on a Mott-insulating initial state ($U = 5$, $\beta = 5$), with different pump-frequencies but an equal amount of absorbed energy ($\Omega = \pi U/4$ and $\Omega = \pi U/2$, $T_{\text{eff}} = 0.5$). The photoemission spectrum $I(\omega, t_p)$ [Eq. 15)] is broadened due to a relatively short pulse duration $\delta = 2$, but the Hubbard bands and a gap can still clearly be distinguished. Similar to the slow relaxation of the double

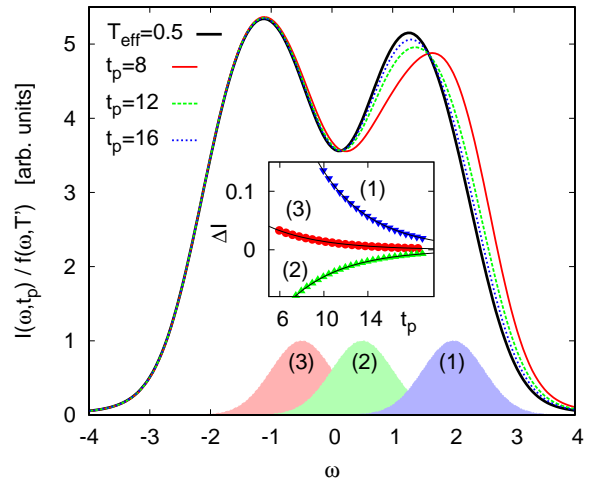


FIG. 4: Time-resolved photoemission spectrum [Gaussian probe, $\delta = 2$] of a pump-excited system ($U = 2.5$, $\beta = 5$), using the pump parameters of Fig. 2a ($\Omega = 5\pi/4$, $E_0 = 1.9123$). Main plot: $I(\omega, t_p)$ for various probe-times t_p , compared to the spectrum $I_{T_{\text{eff}}}(\omega)$ of the equilibrium state at $T_{\text{eff}} = 0.5$. For better visibility of the upper Hubbard band, data have been divided by a Fermi-function with temperature $T' = 0.55$. (T' is chosen by hand and is slightly larger than T_{eff} , in order to account for the broadening effect due to the finite pulse duration.) Inset: Relative difference $I(\omega, t_p)$ to $I_{T_{\text{eff}}}(\omega)$ as a function of t_p , for three probe frequencies $\omega_{(1)} = 2$, $\omega_{(2)} = 0.5$, $\omega_{(3)} = -0.5$. Solid lines show exponential fits $I_{\Omega}(\omega) - I_{T_{\text{eff}}}(\omega) \propto \exp(-t/\tau_{\text{th}})$, with parameters $\tau_{\text{th}} = 4.70$ ($\omega_{(1)}$), 4.82 ($\omega_{(2)}$), 4.77 ($\omega_{(3)}$).

occupancy at $U = 5$, $I(\omega, t_p)$ becomes almost independent of t_p after the decay of the initial transient for all times accessible with the OCA impurity solver. In the figure, we compare the spectra of the pump-excited system at $t_p = 10$ to equilibrium spectra both at the initial temperature ($T = 0.2$) and at $T = T_{\text{eff}}$. The relative differences between these curves are most pronounced in the upper Hubbard band (UHB). Due to thermal fluctuations, the latter acquires much more weight for $T = T_{\text{eff}}$ than for the initial equilibrium state $T = 0.2$. For the two pump-excited states, the weight of the UHB is comparable to the weight of the UHB at $T = T_{\text{eff}}$, but its distribution depends on the pumping process in such a way that the spectral density at high energies is increased for the high-frequency pump.

The differences between the curves in Fig. 3 clearly confirm the nonthermal nature of the excited states, which had already been deduced from the value of the double occupancy. However, a thermal state at $T = T_{\text{eff}}$ might not be accessible in a typical pump-probe experiment, because electronic temperatures can be so high that heating the whole sample to those temperatures would result in its destruction, or at least in a strong modification of its properties. It is thus important to note that no quantitative comparison to the thermal state at

$T = T_{\text{eff}}$ is required in order to identify a lack of thermalization of the electrons, but it is enough to demonstrate that a state still has detailed memory on the way it was prepared. In the present case this memory becomes evident from the fact that the spectral weight distribution depends on the pump-frequency, for systems which have absorbed the same amount of energy.

At intermediate coupling, the time-evolution of the double occupancy has indicated a more rapid thermalization of the system, and we will now demonstrate that this result is confirmed by the behavior of the spectral function. For this purpose we choose a state in the crossover regime ($U = 2.5$, $\beta = 5$), excite it by a pulse of frequency $\Omega = U\pi/2$ to the energy corresponding to $T_{\text{eff}} = 0.5$, and compare the spectrum $I(\omega, t_p)$ to the spectrum $I_{T_{\text{eff}}}(\omega)$ of the thermal equilibrium state at $T = T_{\text{eff}}$ (Fig. 4). At these parameters, the Mott gap is already closed, but the Hubbard bands are still separated by a dip in the spectral function. In the photoemission spectrum, the UHB appears merely as a shoulder on the upper edge, but it can be enhanced by dividing the spectrum by a Fermi function. For small probe-times, $I(\omega, t_p)$ differs from $I_{T_{\text{eff}}}(\omega)$ by a shift of the UHB to larger frequencies, but in contrast to the results for $U = 5$ we now observe a relaxation of the spectrum towards the thermal equilibrium spectrum at later t_p . In the inset of Fig. 4 we plot the relative difference $\Delta I = [I(\omega, t_p) - I_{T_{\text{eff}}}(\omega)]/I_{T_{\text{eff}}}(\omega)$ as a function of probe time t_p for three frequencies, $\omega_{(1)} = 2$ (above the center of the UHB), $\omega_{(2)} = 0.5$ (below the center of the UHB), and $\omega_{(3)} = -0.5$. Due to the shift of spectral weight from higher to lower frequencies, $I(\omega_{(1)}, t_p)$ decreases with t_p , while $I(\omega_{(2)}, t_p)$ increases. A fit of the curves with an exponential decay gives relaxation times $\tau_{\text{th}} = 4.70$ for $\omega_{(1)}$, $\tau_{\text{th}} = 4.82$ for $\omega_{(2)}$, and $\tau_{\text{th}} = 4.77$ for $\omega_{(3)}$, comparable to the relaxation time extracted from $d(t)$ for the same parameters, $\tau_{\text{th}} = 4.87$ (Fig. 2).

V. CONCLUSION

In conclusion, we have investigated the relaxation of a Mott insulator subsequent to a strong laser excitation over the Hubbard gap. After an initial strongly damped transient, the time-evolution of the double occupancy turns into an exponential relaxation towards its thermalized value at large times. For $U \gg W$, the thermalization time grows rapidly with U/W , consistent with the exponentially small decay rate for one doublon in front of a background of singly occupied sites and holes.³² When U is comparable to W , on the other hand, the double occupancy thermalizes within a few times the inverse bandwidth. This more efficient thermalization does not only become manifest through a decrease of the thermalization rate $1/\tau_{\text{th}}$, but moreover, the system approaches a point at which the exponential relaxation is entirely absent, and the thermal state is approached along a qualitatively different, “rapid” pathway.

Exponential thermalization arises when the relevant kinetic equations can be linearized around the thermal state, i.e., when relaxation close to a thermal equilibrium state is described in terms of small deviations from that state. The fact that the long-time relaxation of the double occupancy can be understood from the decay rate of single doublons fits into this scheme. On the other hand, the appearance of the rapid thermalization instead of the exponential relaxation is quite remarkable, in particular as it appears at a value of U that is far from any known phase transition in equilibrium. It remains to be seen whether similar results can be obtained for weak coupling (which is not accessible with the impurity solver used in this work), where the long-time behavior should be described by a Boltzmann equation,¹⁶ and whether it is related to the “rapid thermalization” at the dynamical transition after an interaction quench in the Hubbard model. In any case, the analysis of the long-time tail in terms of the “residue” d_0 used in this paper allows to rigorously define a “rapid thermalization”, and thus should be useful for a future analysis of the dynamical transition after the interaction quench in the Hubbard model and other models.

In this work we have also demonstrated that the differences in thermalization behavior are in principle observable by means of time-resolved photoemission spectroscopy. Quantitative differences between the time-dependent spectrum and equilibrium spectra are small, but nonthermal behavior of the pump-excited system may also be detected from qualitative features, such as the memory of the electronic system on the precise form of the excitation. We suppose that similar information can be drawn from optical measurements, since both the conductivity and the photoemission spectrum are derived from the same single-particle Green function (up to vertex corrections which can be controlled to some extent by varying the relative polarization of pump and probe).³⁵ Of course, most materials are more complicated than the simple one-band Hubbard model studied in this work. But our results suggest that a similar pronounced dependence of the relaxation on the interaction parameter occurs in more complex models. For example, it would be interesting to see whether the relaxation of photo-doped metallic phases to insulating phases in charge transfer insulators¹ is subject to a similar strong dependence on the system parameters as the thermalization of doublons in the half-filled single-band system.

Acknowledgements

We thank M. Kollar, C. Kollath, T. Oka, L. Tarruell, and N. Tsuji for useful discussions. Numerical calculations were run on the Brutus cluster at ETH Zurich. We acknowledge support from the Swiss National Science Foundation (Grant PP002-118866).

-
- ¹ S. Iwai, M. Ono, A. Maeda, H. Matsuzaki, H. Kishida, H. Okamoto, and Y. Tokura, *Phys. Rev. Lett.* **91**, 057401 (2003).
- ² L. Perfetti, P. A. Loukakos, M. Lisowski, U. Bovensiepen, H. Berger, S. Biermann, P. S. Cornaglia, A. Georges, and M. Wolf, *Phys. Rev. Lett.* **97**, 067402 (2006); *New J. of Phys.* **10**, 053019 (2008).
- ³ M. Rini, R. Tobey, N. Dean, J. Itatani, Y. Tomioka, Y. Tokura, R. W. Schoenlein, and A. Cavalleri, *Nature* **449**, 72 (2007).
- ⁴ S. Wall, D. Brida, S. R. Clark, H. P. Ehrke, D. Jaksch, A. Ardavan, S. Bonora, H. Uemura, Y. Takahashi, T. Hasegawa, H. Okamoto, G. Cerullo, and A. Cavalleri, *Nature Physics* **7**, 114 (2011).
- ⁵ N. Dean, J. C. Petersen, D. Fausti, R. I. Tobey, S. Kaiser, L. V. Gasparov, H. Berger, and A. Cavalleri, *Phys. Rev. Lett.* **106**, 016401 (2011).
- ⁶ H. Ichikawa, Sh. Nozawa, T. Sato, A. Tomita, K. Ichiyangi, M. Chollet, L. Guerin, N. Dean, A. Cavalleri, Sh. Adachi, T. Arima, H. Sawa, Y. Ogimoto, M. Nakamura, R. Tamaki, K. Miyano, and Sh. Koshihara, *Nature Materials* **10**, 101 (2011).
- ⁷ P. B. Allen, *Phys. Rev. Lett.* **59**, 1460 (1987).
- ⁸ W. S. Fann, R. Storz, H. W. K. Tom, and J. Bokor, *Phys. Rev. Lett.* **68**, 2834 (1992); *Phys. Rev. B* **46**, 13592 (1992).
- ⁹ M. Greiner, O. Mandel, T. W. Hänsch, and I. Bloch, *Nature* **419**, 51 (2002).
- ¹⁰ T. Kinoshita, T. Wenger, and D. S. Weiss, *Nature* **440**, 900 (2006).
- ¹¹ For recent reviews, see J. Dziarmaga, *Adv. in Phys.* **59**, 1063 (2010); A. Polkovnikov, K. Sengupta, A. Silva, and M. Venkatachalan, arXiv:1007.5331; M. Rigol, arXiv:1008.1930.
- ¹² C. Kollath, A. M. Läuchli, and E. Altman, *Phys. Rev. Lett.* **98**, 180601 (2007).
- ¹³ P. Barmettler, M. Punk, V. Gritsev, E. Demler, and E. Altman, *Phys. Rev. Lett.* **102**, 130603 (2009).
- ¹⁴ M. Eckstein, M. Kollar, and P. Werner, *Phys. Rev. Lett.* **103**, 056403 (2009).
- ¹⁵ M. Eckstein, M. Kollar, and P. Werner, *Phys. Rev. B* **81**, 115131 (2010).
- ¹⁶ M. Möckel and S. Kehrein, *Phys. Rev. Lett.* **100**, 175702 (2008); *Ann. Phys.* **324**, 2146 (2009).
- ¹⁷ M. Rigol, V. Dunjko, V. Yurovsky, and M. Olshanii, *Phys. Rev. Lett.* **98**, 050405 (2007).
- ¹⁸ M. Kollar, F. A. Wolf, and M. Eckstein, arXiv:1102.2117.
- ¹⁹ A. Georges, G. Kotliar, W. Krauth, and M. J. Rozenberg, *Rev. Mod. Phys.* **68**, 13 (1996).
- ²⁰ W. Metzner and D. Vollhardt, *Phys. Rev. Lett.* **62**, 324 (1989).
- ²¹ P. Schmidt and H. Monien, arXiv:cond-mat/0202046 (unpublished); P. Schmidt, Diploma thesis, University of Bonn (1999).
- ²² J. K. Freericks, V. M. Turkowski, and V. Zlatić, *Phys. Rev. Lett.* **97**, 266408 (2006); J. K. Freericks, *Phys. Rev. B* **77**, 075109 (2008).
- ²³ P. Werner, T. Oka and A. J. Millis, *Rev. B* **79**, 035320 (2009).
- ²⁴ N. Tsuji, T. Oka, Ph. Werner, and H. Aoki, arXiv:1008.2594.
- ²⁵ N. Eurich, M. Eckstein, and Philipp Werner, arXiv:1010.2853.
- ²⁶ Ch. Jung, A. Wilhelm, H. Hafermann, S. Brener, and A. Lichtenstein, arXiv:1102.3279.
- ²⁷ M. Eckstein and Ph. Werner, *Phys. Rev. B* **82**, 115115 (2010).
- ²⁸ H. Keiter and J. C. Kimball, *Intern. J. Magnetism* **1**, 233 (1971); *J. Appl. Phys.* **42**, 1460 (1971); N. Grewe and H. Keiter, *Phys. Rev. B* **24**, 4420 (1981); Y. Kuramoto, *Z. Phys. B* **53**, 37 (1983).
- ²⁹ For an introduction into the Keldysh formalism, see R. van Leeuwen, N. E. Dahlen, G. Stefanucci, C.-O. Almbladh and U. von Barth, arXiv:cond-mat/0506130 (published in: *Time-dependent density functional theory*, M. A. L. Marques, C. A. Ullrich, F. Nogueira, A. Rubio, K. Burke, and E. K. U. Gross (eds.), *Lecture Notes in Physics* **706**, Springer, Berlin 2006).
- ³⁰ M. Eckstein, T. Oka, and Ph. Werner, *Phys. Rev. Lett.* **105**, 146404 (2010).
- ³¹ A. Rosch, D. Rasch, B. Binz, and M. Vojta, *Phys. Rev. Lett.* **101**, 265301 (2008).
- ³² R. Sensarma, D. Pekker, E. Altman, E. Demler, N. Strohmaier, D. Greif, R. Jördens, L. Tarruell, H. Moritz, and T. Esslinger, *Phys. Rev. B* **82**, 224302 (2010).
- ³³ J. K. Freericks, H. R. Krishnamurthy, and T. Pruschke, *Phys. Rev. Lett.* **102**, 136401 (2009).
- ³⁴ M. Eckstein and M. Kollar, *Phys. Rev. B* **78**, 245113 (2008).
- ³⁵ M. Eckstein and M. Kollar, *Phys. Rev. B* **78**, 205119 (2008).